npj computational materials

www.nature.com/npjcompumats

ARTICLE OPEN

Check for updates

Atomic coordination dictates vibrational characteristics and thermal conductivity in amorphous carbon

Ashutosh Giri[1]✉, Connor J. Dionne[1] and Patrick E. Hopkins[2,3,4]✉

We discuss the role of atomic coordination in dictating the vibrational characteristics and thermal conductivity in amorphous carbon. Our systematic atomistic simulations on amorphous carbon structures at varying mass densities show the significant role played by the ratio of sp^2 to sp^3 hybridized bonds in dictating the contributions from propagating (phonon-like) and non-propagating vibrational modes and their influence on the overall thermal conductivities of the structures. Specifically, our results show that as the concentration of sp^3-bonded carbon atoms increases, the thermal conductivity can be increased by four fold, which is attributed to enhanced contributions from propagating modes in these amorphous structures. Our results shed more light into the role of atomic coordination on dictating heat transfer mechanisms in amorphous materials, and also provide a deeper understanding of the ability to tune the thermal conductivity of amorphous carbon structures through the control of the local atomic coordination.

npj Computational Materials (2022)8:55 ; https://doi.org/10.1038/s41524-022-00741-7

INTRODUCTION

Diamond-like carbon is a class of amorphous carbon material that has attracted much attention over more than half a century due to it's unique combination of properties that are tunable between those found in diamond and those in graphite[1]. Depending on the sp^3 content in amorphous carbon, the chemical and physical properties can be controlled over a wide range[2,3]. For example, compressing glassy carbon (with nearly 100% sp^2 bonding) to form a new carbon allotrope with a fully sp^3 bonded amorphous structure demonstrated diamond-like extraordinary hardness[4]. Due to such exceptional properties, these materials have found applications in protective and wear resistant coatings[5–7], magnetic storage media[8,9], wide-bandgap semiconductors[10], and carbon-based micro-electro-mechanical systems to name a few[11]. Heat management in some of these applications, however, becomes a major bottleneck to the device efficiency, and fully understanding thermal transport in amorphous carbon layers used in various devices (from a microstructural perspective) becomes increasingly crucial, especially as the thicknesses of these layers continue to decrease[12].

There has been a considerable amount of interest in understanding thermal transport properties in amorphous carbon both from experimental and computational standpoints[3,13–19]. Morath et al.[13] experimentally measured the thermal conductivity of amorphous carbon films in the range of 3–10 $W\,m^{-1}\,K^{-1}$, which are higher in comparison to other amorphous solids and much higher than the corresponding predictions from a minimum thermal conductivity model[14]. They attributed the wide range in their measured values to a potentially long-range order that could result from the formation of microcrystallites for their samples with higher thermal conductivity. Similarly, Shamsa et al.[15] and Bullen et al.[17] have shown that for diamond-like carbon films, thermal conductivity scales linearly with both sp^3 content and the amount of (nano)-crystallinity in the samples. More recently, Scott et al.[16] have also shown that for fully disordered hydrogenated amorphous carbon films (with comparatively lower mass densities ~1.4 $g\,cm^{-3}$ than diamond-like carbon), higher concentrations of sp^3 bonded carbon led to higher measured thermal conductivities.

In line with these experimental results, molecular dynamics (MD) simulations conducted on amorphous carbon structures by Suarez-Martinez et al.[20] demonstrated a monotonic increase in thermal conductivity of amorphous carbon with mass densities ranging from 1.4 to 3 $g\,cm^{-3}$. In MD simulations, an increase in mass density usually results in an increase in the sp^3 content for amorphous carbon structures[21]. Thus, most of these aforementioned works lead to the conclusion that an increase in sp^3 content will result in higher thermal conductivities in disordered carbon. However, a systematic study focusing on the influence of relative fractions of sp^3- and sp^2-bonded carbons on the thermal transport properties of amorphous carbon structures is still missing. Moreover, it is also not clear what impact carbon hybridization has on the fundamental character of the different vibrational modes in amorphous carbon. For example, in amorphous materials where the normal modes of vibrations are categorized into propagons (that are phonon-like and propagating modes), diffusons (that are delocalized but non-propagating), and locons (that are localized modes)[22], what influence does varying the sp^3 content have on the relative contribution from propagating modes in diamond-like carbon structures? We seek to provide insight into these unanswered questions through systematic atomistic simulations in this work.

In general, for amorphous solids it is conventionally assumed that energy transport is limited to the random walk of vibrations, which effectively restricts the mean-free paths of the energy carriers to the order of the average atomic spacing[23]. Therefore, manipulating the thermal conductivity of amorphous solids below the so-called 'minimum limit' has proven challenging since reducing the thermal conductivity would entail constraining the already spatially limited distances of vibrational energy transfer[24]. Recently, however, experimental measurements of thermal

[1]Department of Mechanical, Industrial and Systems Engineering, University of Rhode Island, Kingston, RI 02881, USA. [2]Department of Mechanical and Aerospace Engineering, University of Virginia, Charlottesville, VA 22904, USA. [3]Department of Materials Science and Engineering, University of Virginia, Charlottesville, VA 22904, USA. [4]Department of Physics, University of Virginia, Charlottesville, VA 22904, USA. ✉email: ashgiri@uri.edu; phopkins@virginia.edu

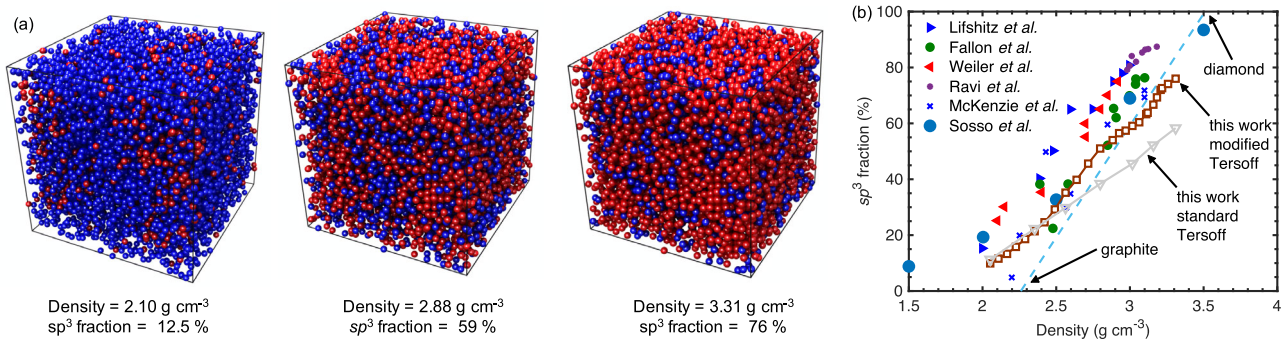

Fig. 1 Concentration of sp^3-bonded carbon atoms in amorphous carbon at different mass densities. a Schematic of our amorphous carbon computational domains showing different ratios of sp^2 to sp^3 hybridized carbon atoms at three representative mass densities; the red atoms correspond to sp^3-bonded carbon atoms with a four-fold coordination. **b** Percentage of sp^3-bonded carbon atoms in the amorphous structures as a function of the mass density showing a linear increase with increasing density for structures described by both the standard and the modified Tersoff potentials. In comparison to the experimental measurements and results from density functional theory calculations, the modified Tersoff potential (with a larger cutoff distance of 2.45 Å) is better able to predict the correct sp^3-bonded carbon fraction in the amorphous structures, especially at higher densities[62–67].

conductivity on amorphous silicon have shown that a significant proportion of the heat is carried by phonon-like vibrations[25–28]. In support of these experiments, atomistic simulations from Larkin et al.[29] quantified the substantial role of propagating modes in amorphous silicon. These recent studies highlight the prospect of tuning the thermal conductivity of amorphous materials through the scattering of long-wavelength propagating modes via nanostructuring, which has been an effective way to tune the thermal conductivity of crystalline solids (by orders of magnitude compared to the bulk value) via phonon scattering from nanostructures and boundaries[30–32]. Along with nanostructuring, recent theoretical and experimental studies have also highlighted the role of chemical disorder through variations in the local bonding environments in crystalline solids as an efficient 'knob' for large reductions in thermal conductivity[33–36]. For example, Lory et al.[34] have shown that in structurally complex materials such as clathrates, reduced acoustic phonon lifetimes resulting from chemical disorder lead to ultra-low thermal conductivities in these crystalline materials. Taken together, the application of the well-established phonon scattering mechanisms and manipulation of local bond disorder in crystalline solids to amorphous solids could be highly beneficial for a variety of applications such as in thermoelectrics, thermal barriers coatings, and microelectronics with multiple amorphous dielectric layers where manipulating thermal transport becomes quintessential[37–39].

Here, we show that propagons can contribute as much as 85% of the total thermal conductivity of amorphous carbon structures, which is the highest propagon contribution in any known fully amorphous solid. We attribute this to the significant proportion of sp^3-bonded carbon atoms in the structures. Through correctly describing the microstructure of the amorphous carbon domain, our MD simulations in conjunction with lattice dynamics (LD) calculations show that increasing the sp^3 content from ~40% to 80% can result in the gradual increase of propagon contribution to the total thermal conductivity from ~50% to 85%. Furthermore, our results show that varying the density of amorphous carbon (and therefore the bond hybridization) can be used as an effective way to tune the total thermal conductivity of diamond-like amorphous carbon in a wide range from ~2.2 to 11 $W\,m^{-1}\,K^{-1}$.

RESULTS AND DISCUSSIONS

Atomic coordination in amorphous carbon

The sp^3 concentrations in our amorphous carbon structures are calculated by identifying the number of carbon atoms with four-fold coordination. Examples of the computational domains with three different sp^3 bond fractions are shown in Fig. 1a where blue and red atoms correspond to sp^2- and sp^3-bonded carbon, respectively. As our main goal is to understand the role of sp^3 bonding on the heat transfer mechanisms in amorphous carbon, we compare the calculated sp^3 fraction for our structures with those measured by several experiments and predicted by density functional theory calculations in Fig. 1b. Although the standard Tersoff potential predicts a monotonically increasing sp^3 content with increasing density, a comparison to prior literature suggests that it drastically underestimates the sp^3 fraction at higher mass densities. The modified Tersoff potential, however, is able to better predict the microstructure of amorphous carbon along with capturing the increasing trend in sp^3 content as a function of density as exemplified by the good agreement between the results from our models (hollow squares in Fig. 1b) and those taken from previous literature (solid symbols). We also note that the radial distribution functions calculated for our amorphous structures described by the modified Tersoff potential are similar to that determined experimentally (see Supplementary notes 1). This validates our use of the modified Tersoff potential to predict the microstructure and thus better describe the heat transfer mechanisms in amorphous carbon. It is also interesting to note that at higher densities, the sp^3 concentration predicted by the modified Tersoff potential agrees well with a 'rule of mixtures' relationship between fully sp^2-bonded graphite and sp^3-bonded carbon structures, whereas the standard Tersoff potential drastically under-predicts the sp^3 content with density. We note that recently the use of machine learning-based potentials such as the Gaussian approximation potential has been shown to better predict the lattice constant of a crystalline diamond as compared to other empirical potentials[40]. As such, the development of ML-based potentials specifically for amorphous carbon deserves further consideration but is beyond the scope of the current work.

Thermal conductivity and vibrational characteristics

Figure 2a shows our GK-calculated thermal conductivities as a function of density for structures described by the modified and the standard Tersoff potentials. For comparison, we also plot the experimentally measured thermal conductivities from Morath et al.[13] and Chen et al.[18] for amorphous carbon samples with different densities. We note that our MD calculations are strictly classical in nature and, as such, cannot capture the quantum effects on the modal heat capacities. Therefore, we focus on the qualitative rather than the quantitative agreement between the experimental results and our MD-predicted thermal conductivities for our amorphous structures described by the modified Tersoff potential. More specifically, while the standard Tersoff potential

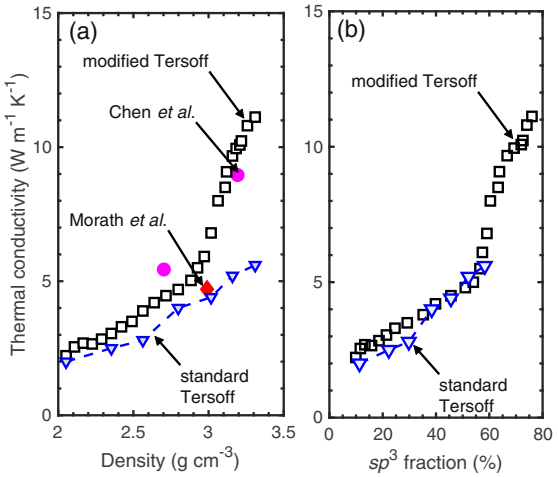

Fig. 2 Thermal conductivity of amorphous carbon. Green-Kubo predicted thermal conductivities of our amorphous carbon domains described by the standard and modified Tersoff potentials at different **a** mass densities and **b** sp^3 content. For comparison, we also include the experimental results from Chen et al.[18] and Morath et al.[13] at the reported densities. While the modified Tersoff potential predicts a higher increase in thermal conductivity at relatively higher mass densities (>2.8 g cm^{-3}), the thermal conductivity of our amorphous carbon structures described by the two potentials are similar when compared to their respective sp^3 concentrations. This suggests that carbon hybridization has a significant role in dictating the thermal conductivity of amorphous carbon.

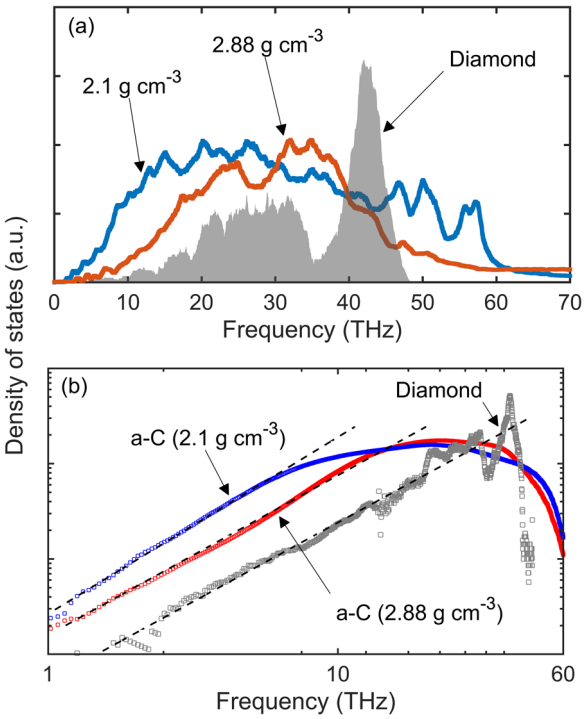

Fig. 3 Vibrational density of states of different carbon structures. **a** Characteristic vibrational density of states, D, showing calculations for high (2.88 g cm^{-3}) and low (2.1 g cm^{-3}) mass density cases for our amorphous carbon structures. For comparison, we also calculate D for a crystalline diamond domain. **b** Lattice dynamics calculated D for the two cases showing the ω^2 scaling at low frequencies. The straight line shows the fit to a Debye model, which is applicable for long-wavelength phonons that propagate with velocities corresponding to the speed of sound in the solid. As the density of our structures decrease, the cutoff frequency where the Debye model is applicable shifts to lower frequencies. For comparison, we also include calculations of D for our crystalline diamond domain where the ω^2 scaling extends to higher frequencies as compared to the amorphous counterparts.

cannot accurately predict the relative increase in thermal conductivity for higher density amorphous carbon structures, the modified Tersoff potential can capture the ~2 × increase in thermal conductivity when the mass density is increased from 3 to 3.2 g cm^{-3}. Overall, for both potentials, the thermal conductivity increases with increasing mass density. For the modified Tersoff case, however, we find a relatively larger increase above densities >3 g cm^{-3} in comparison to the standard Tersoff case. There is a similar trend for the two cases in the increase in sp^3 content with density for domains with densities <2.5 g cm^{-3}, while for domains with densities >2.5 g cm^{-3} the increase in sp^3 content is relatively higher for the modified case (see Fig. 1b). This manifests in the thermal conductivity increase with density for the domains described by the modified Tersoff potential, which are almost a factor of 2 higher than that predicted by the standard Tersoff potential for the highest density cases. However, plotting the thermal conductivities as a function of the sp^3 concentration (as shown in Fig. 2b), the increasing trend for both potentials are similar, which further highlights the significant role played by sp^3 content in dictating the thermal transport in amorphous carbon structures.

Next, to understand the role of carbon hybridization on the vibrational properties, we calculate the vibrational density of states, D, for our various carbon structures at different mass densities. Figure 3a shows our calculated D for high (2.88 g cm^{-3}) and low (2.1 g cm^{-3}) mass density cases, which are notably different as compared to the D calculated from additional simulations on a crystalline (diamond) domain. Most notably, the sharp peaks in the D for the crystalline domain (especially the high-frequency peak at ~40 THz) are not observed for the amorphous structures. Another aspect worth noting is the fact that for our amorphous structures, the relation between D and frequency for the lower frequency (<20 THz) vibrations deviates from the $D(\omega) \propto \omega^2$, which is clearly evident for the crystalline domain. In the Debye approximation, the relation $D(\omega) \propto \omega^2$ holds and is most applicable to long-wavelength phonons that propagate with velocities corresponding to the speed of sound in the solid[41]. This suggests that the propagating (phonon-like) vibrations in the amorphous phases are restricted to lower frequencies (as compared to their crystalline counterparts) and this is further supported in Fig. 3b, which clearly shows the ω^2-dependent trend (straight lines) at low frequencies for the amorphous structures at the two different densities. The deviation from the Debye approximation and the deviation from the phonon-like characteristics for the vibration in the low and high mass densities cases occur at ~5 and 10 THz, respectively. Moreover, as mass density is increased, the frequency range for the propagating modes increases as well, highlighting the role of density (and therefore the sp^3 content) on the vibrational mode characteristic in amorphous carbon. For comparison, we also include the D calculated for our crystalline (diamond) domain showing a larger range of frequencies that follow the ω^2-dependence.

Contributions from propagons and diffusons

To gain a more in-depth understanding of the role of sp^3 content in dictating the relative contributions from propagating and non-propagating modes, we calculate the diffusivities of the modes for our amorphous carbon structures based on the Allen-Feldman theory. Figure 4a shows our calculated diffusivities for the high (2.88 g cm^{-3}) and low (2.1 g cm^{-3}) mass density cases along with the diffusivities for a Stillinger-Weber amorphous silicon structure

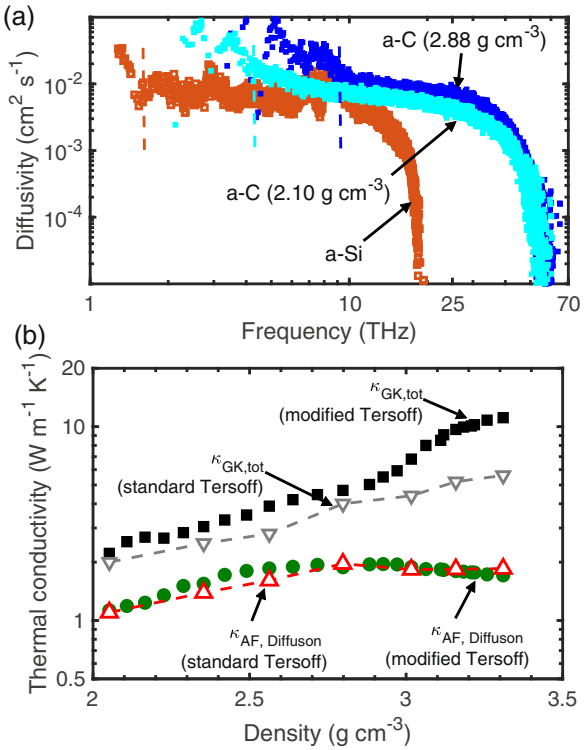

Fig. 4 Diffuson contribution to thermal conductivity in amorphous carbon. a Characteristic mode diffusivity calculations from the Allen and Feldman theory for our amorphous carbon structures with high (2.88 g cm^{-3}) and low (2.1 g cm^{-3}) mass densities. For comparison, the diffusivities for an amorphous silicon domain described by the Stillinger-Weber potential is also included. The dashed lines represent cutoff frequencies for propagating modes below which the diffusivities are relatively higher. **b** Thermal conductivity based on the Allen and Feldman theory for diffusons as a function of mass densities calculated for our amorphous carbon domains described by the standard (red hollow triangles) and modified (green solid circles) Tersoff potentials. For comparison, we also plot the total thermal conductivities predicted from our molecular dynamics simulations based on the Green-Kubo approach.

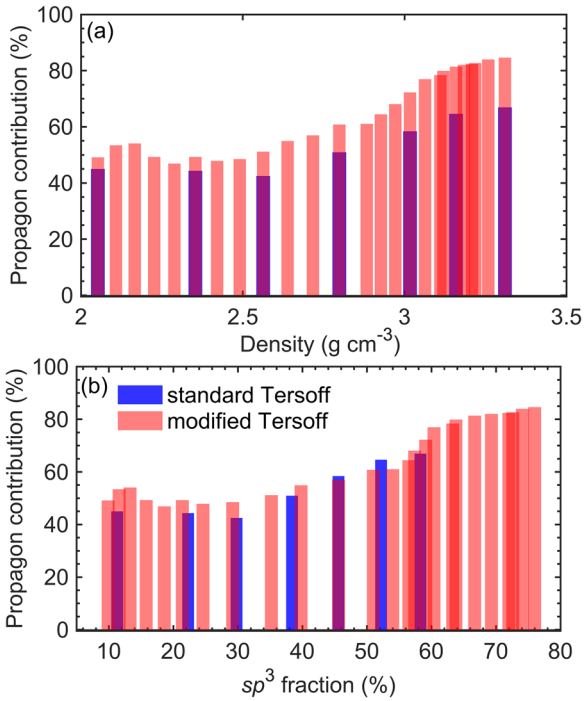

Fig. 5 Propagon contribution to thermal conductivity in amorphous carbon. Estimated propagon contribution to the total thermal conductivity of our amorphous carbon domains as a function of **a** mass densities and **b** fraction of sp^3-bonded carbon atoms.

(calculated from additional simulations)[42]. The sharp decrease in the diffusivities at higher frequencies is indicative of the localized nature of the modes (locons), which do not contribute to the total thermal conductivity directly[43]. For the low-frequency modes (as denoted by the cutoff frequencies signifying the onset of the Debye scaling), diffusivities are relatively larger, which is consistent with their propagating nature. The intermediate frequencies with relatively constant diffusivities are categorized as diffusons for which the contribution to the total thermal conductivity can be calculated by utilizing Eq. (2). Note, the diffusivities of the delocalized modes (diffusons) are higher if the spatial overlap between the eigenvectors are increased as well as if the energetic overlap between the modes are closer to each other. As such, these criterion lead to relatively lower diffusivities for the structures with low densities (<2.5 g cm^{-3}), which are comparable to the diffusivities of modes in our Stillinger-Weber amorphous silicon domain (see Fig. 4a). Therefore, Eq. (2) predicts similar diffuson contributions to the thermal conductivity in the two different structures (~1.1 W m^{-1} K^{-1}).

Figure 4b shows the contribution from the diffusons to the total thermal conductivity for the different amorphous carbon structures described by both the standard and the modified Tersoff potentials. For comparison, we also include the total GK-predicted thermal conductivities for our amorphous carbon structures. Unlike for the total GK-predicted thermal conductivities, the diffuson contribution for both potentials (even at high mass densities) are similar suggesting that the cutoff distance (and the increase in sp^3 content at high mass densities) does not significantly affect our results from the LD calculations. The diffuson thermal conductivity also agrees well with the minimum thermal conductivity model, which assumes that heat is transported through energy carriers with mean-free paths of the order of the average atomic spacing rather than from phonon-like modes (see Supplementary notes 3). For the relatively lower densities (<2.5 g cm^{-3}), both the GK-predicted total thermal conductivity and the diffuson thermal conductivity increase monotonically. For higher mass densities, although the GK-predictions have an increasing trend with mass density, the diffuson contributions are relatively constant at ~1.9 W m^{-1} K^{-1}. Therefore, increasing the density above 2.5 g cm^{-3} increases the contribution from the propagating modes in our amorphous carbon structures while leading to a reduced contribution from the diffusons as the sp^3 content increases in the structures. This is quantitatively shown in Fig. 5a where we plot the propagon contribution (estimated using Eq. (4)) as a function of density of our amorphous structures. For the relatively lower densities (<2.5 g cm^{-3}), the propagon contributions are ~50%, whereas increasing the density above 2.5 g cm^{-3} leads to a gradual enhancement in the contribution of propagons (for structures described by both the standard and the modified Tersoff potentials). The modified potential leads to a ~85% contribution for the propagating modes while for the standard Tersoff potential, the contribution from propagons reaches ~65% for mass densities of 3.4 g cm^{-3}. However, plotting the propagon contribution as a function of sp^3 content (Fig. 5b) shows that the predictions from the two potentials agree well, suggesting that one of the significant factors in controlling the propagon contributions in amorphous carbon is atomic coordination.

From our additional calculations on the amorphous Stillinger-Weber silicon domain, we estimate ~27% contribution from propagons using Eq. (4), which is in good agreement with prior works[44,45]. The relatively higher contribution from propagons in amorphous carbon structures as compared to amorphous silicon can be attributed to the stiffer bonds in the carbon structures that result in higher sound speeds, which dictate the mean-free-paths of the propagating modes (as $\kappa_{pr} \propto v_s^2$)[29]. Recently, Liao et al.[45] have also shown that propagon contribution in amorphous silicon nitride can be as high as 70%, which is more than 2 × the contribution of propagons in amorphous Stillinger-Weber silicon. They attribute the higher propagating mode contributions to higher sound velocities in amorphous silicon nitride. As we have shown in this work, by tuning the sp^3 fraction from ~ 40% to 80%, the contribution from propagons can be varied from ~50 to 85% in amorphous carbon. This is qualitatively in line with the conclusions by Liao et al.[45] due to the fact that the mechanical properties such as the bulk modulus and Young's modulus (and therefore the sound speed) in amorphous carbon have been shown to increase as the fraction of sp^3-bonded carbon increases [21,46].

In summary, we have studied the role of carbon hybridization on the vibrational heat transfer mechanisms in amorphous carbon structures via systematic atomistic simulations. Our results show the significant role played by the fraction of sp^3-bonded carbon atoms in dictating the contributions from propagating (phonon-like) vibrational modes and their influence on the overall thermal conductivity. We have shown that as the concentration of sp^3-bonded carbon atoms increases from ~10 to ~80% in our amorphous carbon structures, the thermal conductivity can be increased by four folds through the drastic increase in the contribution from propagating modes. More specifically, the results from our molecular dynamics simulations in conjunction with our lattice dynamics calculations have shown that as the sp^3 fraction increases from ~40 to 80%, the propagon contribution to the total thermal conductivity can be increased from ~50 to 85%. This is in contrast to the effect of hybridization on the thermal conductivity of modes that are described as diffusons (that are non-propagating modes), which remain relatively constant at high sp^3 fractions. For our amorphous carbon structure with the highest concentration of sp^3-bonded carbon, the thermal conductivity can reach a record high value of 11 W m^{-1} K^{-1}, which is the highest thermal conductivity for any known amorphous solid till date. Our study reveals the relationship between atomic coordination and the fundamental characteristics of the vibrational modes in amorphous carbon, thus opening an avenue to efficiently tune the thermal conductivity of these materials based on carbon hybridization.

METHODS

Computational domain setup

Our amorphous carbon domains are generated with a melt-quench technique by utilizing the standard Tersoff potential[47,48]. As extending the cutoff radius to 2.45 Å in the standard Tersoff potential can correctly locate the second neighbor atomic shell and accurately reproduce the mechanical properties of diamond-like carbon structures[21,49], we also study structures described by this modified potential. Comparing the results between the modified and the standard Tersoff interatomic potentials will also shed more light on the dominant role of sp^3-bonded carbon in the overall thermal conductivity as we detail below. All MD simulations are performed with the LAMMPS package and the General Utility Lattice Program (GULP) is used for the LD calculations[50,51]. Starting with a diamond cubic lattice with a lattice constant of 3.57 Å and periodic boundary conditions applied in all three principal directions, we heat the computational domains at 14,000 K until the atoms lose the memory of their initial positions and structures are completely melted. Rapid quenching is then applied followed by an annealing procedure at 1100 K for a total of 10 ns. This ensures that metastabilities are removed (as evidenced by the potential energy of the system, which does not change with annealing time)[52]. Note, as it has been shown that cooling rates above 10^{16} K/s prevent proper relaxation of the structures resulting in artificially high sp^3 fractions for amorphous carbon, we use a cooling rate ~10^{13} K/s for our structures to ensure proper relaxation. The systems were then equilibrated at 300 K for a total of 2 ns under the isothermal ensemble (NVT integration) with the number of particles, volume, and temperature of the system held constant. By following this procedure and constraining the domains at the prescribed volumes, we can make amorphous carbon structures with mass densities in the range of 2.1–3.4 g cm^{-3}. We also ensure that no voids are formed during the entire equilibration process by monitoring the atomic densities and atomic coordinations in frequent intervals.

Green-Kubo approach

After equilibration, all simulations are run with a 0.25 fs time-step under the microcanonical ensemble (NVE) for a total of 10 ns. To accurately predict the thermal conductivities, we utilize the Green-Kubo (GK) approach[53–59], Under this approach, the thermal conductivity in the αth direction is given by,

$$\kappa_\alpha = \frac{1}{k_B V T^2} \int_0^\infty \langle J_\alpha(t) J_\alpha(0) \rangle dt, \quad (1)$$

where t is the time, T and V are the temperature and volume of the system under consideration, respectively, and $\langle J_\alpha(t) J_\alpha(0) \rangle$ is the αth component of the heat current autocorrelation function (HCACF). Since our structures are amorphous, κ_α predicted in the three principle directions are similar for our structures. Therefore, we report the average thermal conductivity of the three directions. During the data collection period for the GK approach, the HCACF is calculated every 10-time steps. Integration of the HCACF is carried out until it completely decays to zero as shown in Fig. 6a for our amorphous carbon structure with a 3.02 g cm^{-3} mass density described by the standard Tersoff potential. The corresponding thermal conductivity calculated from the integration of the HCACF is shown in Fig. 6b. As the HCACF has clearly decayed to zero from 2 to 7 ps, we average the data for this time period as shown by the dashed line to accurately predict the thermal conductivities of our amorphous carbon structures. The total GK simulation time is set to 5 ns, which is long enough to produce converged thermal conductivities for all our structures. Even though this GK approach has been shown to be a robust method to calculate reliable thermal conductivities[60], size effects can still affect the thermal conductivity calculations if all the vibrational modes are not included in the simulated computational domain[29]. Therefore, we perform simulations on computational domains with different cell lengths, d, to rule outsize effects from our GK thermal conductivity predictions. Figure 6c shows GK-predicted

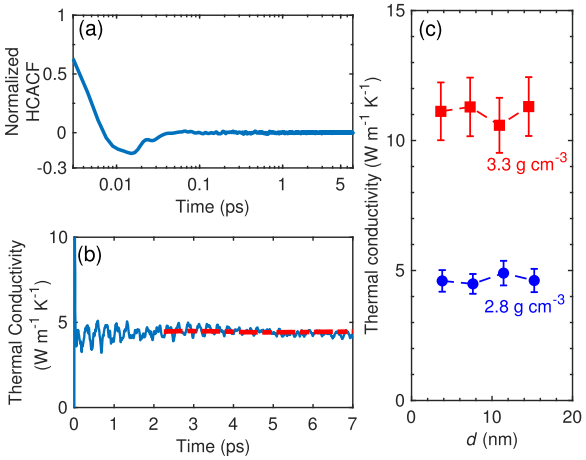

Fig. 6 Green-Kubo approach to predict thermal conductivity of amorphous carbon. Normalized heat current autocorrelation function (HCACF) versus time for our amorphous carbon structure with a mass density of 3.02 g cm^{-3} described by the Tersoff potential. **b** Thermal conductivity is determined from the integration of the HCACF and a converged value is obtained by averaging from 2 to 7 ps integration time. **c** Thermal conductivity as a function of computational domain length, d, for our amorphous carbon structures with 2.8 g cm^{-3} and 3.3 g cm^{-3} as described by the modified Tersoff potential. The error bars represent uncertainties calculated based on results from three independent simulations.

thermal conductivities with varying d for our amorphous carbon domains with 2.8 g cm^{-3} and 3.3 g cm^{-3} mass densities (and as described by the modified Tersoff potential). Within uncertainties (calculated from five independent simulations), the results are similar for all d suggesting that size effects do not influence our reported thermal conductivities for our amorphous structures with computational domain sizes of ~38 × 38 × 38 Å^3. To gain further confidence in our reported values, we run additional nonequilibrium molecular dynamics simulations to show that the thermal conductivity calculated by the direct approach agrees with the GK calculations (see Supplementary notes 2).

Allen-Feldman approach

To get an estimate of the contribution to the total thermal conductivity from the propagating modes and the non-propagating (diffuson) modes, we run LD calculations to quantify the diffuson thermal conductivity. To this end, we calculate the diffusivities of the eigenmodes for our amorphous carbon structures based on the Allen and Feldman (AF) theory[22,61]. The AF-predicted thermal conductivity is given by,

$$\kappa_{\mathrm{AF}} = \sum_{\text{diffusons}} = \frac{k_{\mathrm{B}}}{V} D_{\mathrm{AF},n}(\omega_n), \tag{2}$$

where ω_n is the frequency of the nth diffuson and $D_{\mathrm{AF},n}$ for the harmonic modes is calculated as,

$$D_{\mathrm{AF},n}(\omega_n) = \frac{\pi V^2}{\hbar^2 \omega_n^2} \sum_{m \neq n} |S_{nm}|^2 \delta(\omega_n - \omega_m), \tag{3}$$

where $|S_{nm}|$ is the heat current operator under the harmonic approximation. We note that the Lorentzian broadening of the delta function must be several times greater than the average mode spacing, δ_{avg}. Therefore, for our LD calculations, we set the broadening to $5\delta_{\mathrm{avg}}$ and check for convergence. From the calculation of κ_{AF}, we can estimate the propagon thermal conductivity, κ_{pr} from the relation,

$$\kappa_{\mathrm{total}} = \kappa_{\mathrm{AF}} + \kappa_{\mathrm{pr}}, \tag{4}$$

where we assume κ_{total} as the GK-predicted thermal conductivity. Note, MD simulations inherently contain the contributions from all types propagating and non-propagating modes, thus validating the use of Eq. (4) in estimating the propagon contribution.

The density of states calculations

For the calculation of the vibrational density of states, $D(\omega)$, from our MD simulations, we output the velocities of the carbon atoms every 10-time steps for a total of 1 ns. Following the collection of the velocity-time series, a velocity autocorrelation function (VACF) algorithm is used following a fourier transform ($\mathcal{F}$) of the VACF to obtain the local vibrational $D(\omega)$ as shown in Fig. 3a. More specifically, the Welch method of power spectral density estimation is applied to obtain our $D(\omega)$ as follows,

$$D(\omega) = \frac{1}{2} m \mathcal{F}(\mathrm{VACF}) \frac{1}{k_{\mathrm{B}} T} \rho \tag{5}$$

where m is the atomic mass, k_{B} is the Boltzmann constant, T is the local temperature, and ρ is the atomic density.

DATA AVAILABILITY

The data supporting the present work are available from the corresponding authors upon reasonable request.

Received: 24 November 2021; Accepted: 17 February 2022;
Published online: 04 April 2022

REFERENCES

1. Lifshitz, Y. Diamond-like carbon—present status. *Diam. Relat. Mater.* **8**, 1659–1676 (1999).
2. Casiraghi, C., Robertson, J. & Ferrari, A. C. Diamond-like carbon for data and beer storage. *Mater. Today* **10**, 44–53 (2007).
3. Balandin, A. A., Shamsa, M., Liu, W. L., Casiraghi, C. & Ferrari, A. C. Thermal conductivity of ultrathin tetrahedral amorphous carbon films. *Appl. Phys. Lett.* **93**, 043115 (2008).
4. Lin, Y. et al. Amorphous diamond: a high-pressure superhard carbon allotrope. *Phys. Rev. Lett.* **107**, 175504 (2011).
5. Robertson, J. Ultrathin carbon coatings for magnetic storage technology. *Thin Solid Films* **383**, 81–88 (2001).
6. Rottmayer, R. et al. Heat-assisted magnetic recording. *IEEE Trans. Magn.* **42**, 2417–2421 (2006).
7. Li, X., Wang, A. & Lee, K.-R. Mechanism of contact pressure-induced friction at the amorphous carbon/alpha olefin interface. *npj Comput. Mater.* **4**, 53 (2018).
8. Xu, B. et al. HAMR media design in optical and thermal aspects. *IEEE Trans. Magn.* **49**, 2559–2564 (2013).
9. Kryder, M. et al. Heat assisted magnetic recording. *Proc. IEEE* **96**, 1810–1835 (2008).
10. Tibrewala, A., Peiner, E., Bandorf, R., Biehl, S. & Lüthje, H. Transport and optical properties of amorphous carbon and hydrogenated amorphous carbon films. *Appl. Surf. Sci.* **252**, 5387–5390 (2006).
11. Peiner, E. et al. Diamond-like carbon for MEMS. *J. Micromech. Microeng.* **17**, S83–S90 (2007).
12. Shi, L. et al. Evaluating broader impacts of nanoscale thermal transport research. *Nanoscale Microscale Thermophys. Eng.* **19**, 127–165 (2015).
13. Morath, C. J. et al. Picosecond optical studies of amorphous diamond and diamondlike carbon: thermal conductivity and longitudinal sound velocity. *J. Appl. Phys.* **76**, 2636–2640 (1994).
14. Cahill, D. G., Watson, S. K. & Pohl, R. O. Lower limit to the thermal conductivity of disordered crystals. *Phys. Rev. B* **46**, 6131–6140 (1992).
15. Shamsa, M. et al. Thermal conductivity of diamond-like carbon films. *Appl. Phys. Lett.* **89**, 161921 (2006).
16. Scott, E. A. et al. Thermal conductivity enhancement in ion-irradiated hydrogenated amorphous carbon films. *Nano Lett.* **21**, 3935–3940 (2021).
17. Bullen, A. J., O'Hara, K. E., Cahill, D. G., Monteiro, O. & von Keudell, A. Thermal conductivity of amorphous carbon thin films. *J. Appl. Phys.* **88**, 6317–6320 (2000).
18. Chen, G., Hui, P. & Xu, S. Thermal conduction in metalized tetrahedral amorphous carbon (ta–c) films on silicon. *Thin Solid Films* **366**, 95–99 (2000).
19. Lv, W. & Henry, A. Phonon transport in amorphous carbon using Green–Kubo modal analysis. *Appl. Phys. Lett.* **108**, 181905 (2016).
20. Suarez-Martinez, I. & Marks, N. A. Effect of microstructure on the thermal conductivity of disordered carbon. *Appl. Phys. Lett.* **99**, 033101 (2011).
21. Sha, Z., Branicio, P., Pei, Q., Sorkin, V. & Zhang, Y. A modified tersoff potential for pure and hydrogenated diamond-like carbon. *Comput. Mater. Sci.* **67**, 146–150 (2013).
22. Allen, P. B. & Feldman, J. L. Thermal conductivity of disordered harmonic solids. *Phys. Rev. B* **48**, 12581–12588 (1993).
23. Einstein, A. Elementare betrachtungen uber die thermische molekularbewegung in festen korpern. *Ann. Phys.* **340**, 679 (1911).
24. Braun, J. L. et al. Breaking network connectivity leads to ultralow thermal conductivities in fully dense amorphous solids. *Appl. Phys. Lett.* **109**, 191905 (2016).
25. Braun, J. L. et al. Size effects on the thermal conductivity of amorphous silicon thin films. *Phys. Rev. B* **93**, 140201 (2016).
26. Regner, K. T. et al. Broadband phonon mean free path contributions to thermal conductivity measured using frequency domain thermoreflectance. *Nat. Commun.* **4**, 1640 (2013).
27. Kwon, S., Zheng, J., Wingert, M. C., Cui, S. & Chen, R. Unusually high and anisotropic thermal conductivity in amorphous silicon nanostructures. *ACS Nano* **11**, 2470–2476 (2017).
28. Zhou, C. et al. Enhanced reduction of thermal conductivity in amorphous silicon nitride-containing phononic crystals fabricated using directed self-assembly of block copolymers. *ACS Nano* **14**, 6980–6989 (2020).
29. Larkin, J. M. & McGaughey, A. J. H. Thermal conductivity accumulation in amorphous silica and amorphous silicon. *Phys. Rev. B* **89**, 144303 (2014).
30. Yu, J.-K., Mitrovic, S., Tham, D., Varghese, J. & Heath, J. R. Reduction of thermal conductivity in phononic nanomesh structures. *Nat. Nanotechnol.* **5**, 718 (2010).
31. Hopkins, P. E. et al. Reduction in the thermal conductivity of single crystalline silicon by phononic crystal patterning. *Nano Lett.* **11**, 107–112 (2011).
32. Vineis, C. J., Shakouri, A., Majumdar, A. & Kanatzidis, M. G. Nanostructured thermoelectrics: big efficiency gains from small features. *Adv. Mater.* **22**, 3970–3980 (2010).
33. Braun, J. L. et al. Charge-induced disorder controls the thermal conductivity of entropy-stabilized oxides. *Adv. Mater.* **30**, 1805004 (2018).
34. Lory, P.-F. et al. Direct measurement of individual phonon lifetimes in the clathrate compound $Ba_{7.81}Ge_{40.67}Au_{5.33}$. *Nat. Commun.* **8**, 491 (2017).
35. Giri, A., Braun, J. L. & Hopkins, P. E. Reduced dependence of thermal conductivity on temperature and pressure of multi-atom component crystalline solid solutions. *J. Appl. Phys.* **123**, 015106 (2018).
36. Giri, A., Braun, J. L., Rost, C. M. & Hopkins, P. E. On the minimum limit to thermal conductivity of multi-atom component crystalline solid solutions based on impurity mass scattering. *Scr. Mater.* **138**, 134–138 (2017).

37. Zebarjadi, M., Esfarjani, K., Dresselhaus, M. S., Ren, Z. F. & Chen, G. Perspectives on thermoelectrics: from fundamentals to device applications. *Energy Environ. Sci.* **5**, 5147–5162 (2012).
38. Padture, N. P., Gell, M. & Jordan, E. H. Thermal barrier coatings for gas-turbine engine applications. *Science* **296**, 280–284 (2002).
39. Giri, A. et al. Interfacial defect vibrations enhance thermal transport in amorphous multilayers with ultrahigh thermal boundary conductance. *Adv. Mater.* **30**, 1804097 (2018).
40. Qian, C., McLean, B., Hedman, D. & Ding, F. A comprehensive assessment of empirical potentials for carbon materials. *APL Mater.* **9**, 061102 (2021).
41. Kittel, C. *Introduction to Solid State Physics*, 6th edn. (John Wiley & Sons, Inc., 1986).
42. Stillinger, F. H. & Weber, T. A. Computer simulation of local order in condensed phases of silicon. *Phys. Rev. B* **31**, 5262–5271 (1985).
43. Feldman, J. L., Kluge, M. D., Allen, P. B. & Wooten, F. Thermal conductivity and localization in glasses: Numerical study of a model of amorphous silicon. *Phys. Rev. B* **48**, 12589–12602 (1993).
44. Giri, A., Donovan, B. F. & Hopkins, P. E. Localization of vibrational modes leads to reduced thermal conductivity of amorphous heterostructures. *Phys. Rev. Mater.* **2**, 056002 (2018).
45. Liao, Y. & Shiomi, J. Akhiezer mechanism dominates relaxation of propagons in amorphous material at room temperature. *J. Appl. Phys.* **130**, 035101 (2021).
46. Jana, R., Savio, D., Deringer, V. L. & Pastewka, L. Structural and elastic properties of amorphous carbon from simulated quenching at low rates. *Modell. Simul. Mater. Sci. Eng.* **27**, 085009 (2019).
47. Tersoff, J. New empirical approach for the structure and energy of covalent systems. *Phys. Rev. B* **37**, 6991–7000 (1988).
48. Tersoff, J. Modeling solid-state chemistry: Interatomic potentials for multicomponent systems. *Phys. Rev. B* **39**, 5566–5568 (1989).
49. Titantah, J. & Lamoen, D. sp3/sp2 characterization of carbon materials from first-principles calculations: X-ray photoelectron versus high energy electron energy-loss spectroscopy techniques. *Carbon* **43**, 1311–1316 (2005).
50. Plimpton, S. Fast parallel algorithms for short-range molecular dynamics. *J. Comput. Phys.* **117**, 1–19 (1995).
51. Gale, J. D. & Rohl, A. L. The general utility lattice program (gulp). *Mol. Simul.* **29**, 291–341 (2003).
52. Feldman, J. L., Allen, P. B. & Bickham, S. R. Numerical study of low-frequency vibrations in amorphous silicon. *Phys. Rev. B* **59**, 3551–3559 (1999).
53. Allen, M. P. & Tildesley, D. J. *Computer Simulation of Liquids (Oxford Science Publications)* Reprint edn. (Oxford University Press, 1989).
54. Schelling, P. K., Phillpot, S. R. & Keblinski, P. Comparison of atomic-level simulation methods for computing thermal conductivity. *Phys. Rev. B* **65**, 144306 (2002).
55. McGaughey, A. & Kaviany, M. Thermal conductivity decomposition and analysis using molecular dynamics simulations: Part ii. complex silica structures. *Int. J. Heat. Mass Transf.* **47**, 1799–1816 (2004).
56. McGaughey, A. & Kaviany, M. Thermal conductivity decomposition and analysis using molecular dynamics simulations. part i. lennard-jones argon. *Int. J. Heat. Mass Transf.* **47**, 1783–1798 (2004).
57. Giri, A. & Hopkins, P. E. Pronounced low-frequency vibrational thermal transport in c_{60} fullerite realized through pressure-dependent molecular dynamics simulations. *Phys. Rev. B* **96**, 220303 (2017).
58. Giri, A. et al. Molecular tail chemistry controls thermal transport in fullerene films. *Phys. Rev. Mater.* **4**, 065404 (2020).
59. Giri, A. & Hopkins, P. E. Resonant phonon modes in fullerene functionalized graphene lead to large tunability of thermal conductivity without impacting the mechanical properties. *J. Appl. Phys.* **125**, 205102 (2019).
60. Wang, Z., Safarkhani, S., Lin, G. & Ruan, X. Uncertainty quantification of thermal conductivities from equilibrium molecular dynamics simulations. *Int. J. Heat. Mass Transf.* **112**, 267–278 (2017).
61. Larkin, J. M. & McGaughey, A. J. H. Predicting alloy vibrational mode properties using lattice dynamics calculations, molecular dynamics simulations, and the virtual crystal approximation. *J. Appl. Phys.* **114**, 023507 (2013).
62. Grossman, E. et al. Role of ion energy in determination of the sp3 fraction of ion beam deposited carbon films. *Appl. Phys. Lett.* **68**, 1214–1216 (1996).
63. Fallon, P. J. et al. Properties of filtered-ion-beam-deposited diamondlike carbon as a function of ion energy. *Phys. Rev. B* **48**, 4777–4782 (1993).
64. Weiler, M. et al. Highly tetrahedral, diamond-like amorphous hydrogenated carbon prepared from a plasma beam source. *Appl. Phys. Lett.* **64**, 2797–2799 (1994).
65. Ravi, S. et al. Nanocrystallites in tetrahedral amorphous carbon films. *Appl. Phys. Lett.* **69**, 491–493 (1996).
66. Sosso, G. C., Deringer, V. L., Elliott, S. R. & Csányi, G. Understanding the thermal properties of amorphous solids using machine-learning-based interatomic potentials. *Mol. Simul.* **44**, 866–880 (2018).
67. McKenzie, D. et al. Tetrahedral amorphous carbon properties and applications. *J. Non Cryst. Solids* **164-166**, 1101–1106 (1993).

ACKNOWLEDGEMENTS

This work is supported by the Office of Naval Research, Grant Nos. N00014-21-1-2622 and N00014-20-1-2686, and the Semiconductor Research Corporation, Grant No. 2021-NM-3047.

AUTHOR CONTRIBUTIONS

A.G. and P.E.H. conceived the research plan. A.G. and C.J.D. performed the calculations and analysis. A.G. and P.E.H. wrote the manuscript and all authors discussed the results.

COMPETING INTERESTS

The authors declare no competing interests.

ADDITIONAL INFORMATION

Supplementary information The online version contains supplementary material available at https://doi.org/10.1038/s41524-022-00741-7.

Correspondence and requests for materials should be addressed to Ashutosh Giri or Patrick E. Hopkins.

Reprints and permission information is available at http://www.nature.com/reprints

Publisher's note Springer Nature remains neutral with regard to jurisdictional claims in published maps and institutional affiliations.